arXiv:physics/0308054v1 [physics.atom-ph] 14 Aug 2003

Sub-Doppler spectroscopy of Rb atoms in a sub-micron vapor cell in the presence of a magnetic field

David Sarkisyan, Aram Papoyan, Tigran Varzhapetyan

Institute for Physical Research, NAS of Armenia, Ashtarak-2 378410 Armenia

Janis Alnis, Kaspars Blush, Marcis Auzinsh

Department of Physics, University of Latvia,

19 Rainis blvd, Riga, LV-1585, Latvia

(Dated: February 2, 2008)

Abstract

We report the first use of an extremely thin vapor cell (thickness $\sim$ 400 nm) to study the magnetic-field dependence of laser-induced-fluorescence excitation spectra of alkali atoms. This thin cell allows for sub-Doppler resolution without the complexity of atomic beam or laser cooling techniques. This technique is used to study the laser-induced-fluorescence excitation spectra of Rb in a 50 G magnetic field. At this field strength the electronic angular momentum **J** and nuclear angular momentum **I** are only partially decoupled. As a result of the mixing of wavefunctions of different hyperfine states, we observe a nonlinear Zeeman effect for each sublevel, a substantial modification of the transition probabilities between different magnetic sublevels, and the appearance of transitions that are strictly forbidden in the absence of the magnetic field. For the case of right- and left- handed circularly polarized laser excitation, the fluorescence spectra differs qualitatively. Well pronounced magnetic field induced circular dichroism is observed. These observations are explained with a standard approach that describes the partial decoupling of **I** and **J** states.

I. INTRODUCTION

Sub-Doppler probes of atoms and molecules in a thermal gas cell is a well-established subfield of laser spectroscopy. In particular, velocity-selective techniques such as saturated absorption spectroscopy, polarization spectroscopy, Doppler-free two photon spectroscopy [1, 2], coherent dark state spectroscopy [3] and other techniques can provide linewidths orders of magnitude smaller than the Doppler width.

During the past several years a fundamentally different approach has been developed. This new method is based on the spectroscopy of a diluted atomic vapor in an extremely thin cell. In most of these studies thermal Cs atoms are confined to cells of thickness of 10 μm to 1000 μm. The Cs atoms that are moving parallel to the cell walls are laser excited and fluoresce in much the same way as atoms in a normal vapor cell. Atoms moving perpendicularly to the closely-spaced cell walls are likely to suffer collisions with the wall before they absorb and fluoresce and therefore do not make a significant contribution to the laser-induced fluorescence signal. Thus the spectra obtained is that of atoms that show no first-order Doppler shift. This approach allows for a relatively simple experimental apparatus to provide sub-Doppler resolution [4, 5, 6, 7, 8, 9, 10].

It was demonstrated a long time ago in microwave spectroscopy [11], and recently in the optical domain [12, 13, 14, 15], that the optimal cell thickness L for atomic line shape narrowing is approximately $\lambda/2$ where λ is the wavelength of spectral features to be observed. This fact stimulated us (D.S. and A.P.) to develop an extremely thin gas cell of thickness of $100 - 300$ nm. As far as we know this is an absolute record. The cell used in the present investigation is at least one order of magnitude thinner than all other cells used in this manner and has allowed for the first optical measurement of atoms in a cell which satisfies the condition $L \approx \lambda/2$. These conditions allowed recently to resolve all hyperfine transitions of the D_2 line of Cs atoms. In addition to the Cs study, a naturally occurring isotopic mixture of Rb atoms was introduced to the thin cell. For this case, ^{85}Rb and ^{87}Rb hyperfine transitions were well resolved in the first D_1 line fluorescence spectrum [16]. In addition to removing Doppler broadening, thin cells provide a second advantage that is not evident in other types of spectroscopy: In an ordinary vapor cell it is extremely easy to reach laser intensities that change the atomic ground state magnetic sublevel population (optical pumping) and to saturate transitions. In ordinary cells optical pumping of atomic

states typically occurs at laser radiation intensities of $10 - 1000$ nW/cm^2 complicating the experimental determination of relative absorption strengths and/or atomic populations. In a thin cell, however, the population of atoms that do not move parallel to the cell walls constantly replenish depleted ground-state population, leading to linear laser absorption at laser intensities up to at least, 50 mW/cm^2 [16].

In the present paper we demonstrate that a sub-micron cell not only allows for sub-Doppler atomic spectroscopy, but more sophisticated studies of linear magneto-optical effects as well. Specifically, we use sub-micron cells filled with ^{85}Rb and ^{87}Rb to explore circular dichroism induced by an external magnetic field. The effect of magnetic field-induced circular dichroism is important for a variety of reasons. For some time there have been attempts to use polarization plane rotation of a laser beam by an atomic or molecular gas to test of CP parity violation caused by interference between the neutral weak and electromagnetic interactions that couple a valence electron to the nucleus [17, 18, 19, 20]. Alkali atoms including Cs are considered as a perspective objects for such CP parity violation measurements. Simple linear magneto optical effects caused by stray magnetic fields in general and magnetic field induced circular dichroism in particular can mimic the effect of rotation of the laser beam polarization plane by parity-violating neutral currents. It is therefore essential that the less exotic linear magneto-optical effect be completely understood. In a more practical application, magnetic field induced circular dichroism in alkali atoms has been successfully applied for a diode laser frequency stabilization based on difference of the absorption of right-hand and left-hand circular polarized radiation in atomic vapor placed in the constant magnetic field [21, 22]. This technique was applied to diode lasers in the work of the Joint Institute for Laboratory Astrophysics (JILA) group [23] who coined for this stabilization method the term *dichroic atomic vapor laser lock* (DAVLL).

In general circular dichroism studies in alkali metal vapors have a long history. The first detailed study of magneto optical rotational effects for closely lying hyperfine levels were performed in connection with the non-conservation of CP parity in bismuth [24, 25]. The work of G.J. Roberts et al is a combined theoretical and experimental investigation of magneto-optical effects on Doppler broadened transitions [25]. The primary focus of this work is Faraday rotation but the closely related phenomenon of magnetic field induced circular dichroism is discussed as well. The shift of the energy of magnetic sublevels in the magnetic field is considered and hyperfine level mixing caused by the field is taken into

account as well. Doppler broadened optical rotation spectra and, in one experiment, circular dichroism spectra are observed. Typical features of the spectra have widths of the order of GHz. In a more recent paper [26], Doppler broadened magneto-optical rotation spectra in a room-temperature Cs vapor in a magnetic field of the order of 45 G, are presented, along with a corresponding theoretical treatment. An interesting result of the theoretical treatment is the fact that even at this relatively weak magnetic field, the perturbation of the wave function plays an essential role in the Zeeman energy level shift. In a study carried out in Quebec [27] both isotopes of rubidium ^{85}Rb and ^{87}Rb as well as Cs atoms are used to study absorption spectra of atoms in presence of a magnetic field. In this study relatively strong magnetic field strengths of 790, 1440 and 2300 G are applied to the gas cell. It is shown that a magnetic field strength exceeding 1000 G is required to observe magnetic structure in the Doppler broadened absorption spectra. At this high field values hyperfine coupling is broken and nuclear and electronic moments in atom are decouple. Studies of linear magneto-optical methods can be carried out also by non-direct methods like selective reflection spectroscopy [28, 29] but will not be discussed in this work.

In present paper we demonstrate that extremely thin gas cells can be used successfully to study with sub-Doppler resolution magnetic field induced circular dichroism in atoms. We are not aware of any previous experimental study of magnetic field induced circular dichroism that employes a sub-Doppler technique, although a theoretical study of magneto-optical effects on atoms in a thin cell has been carried out previously [13]. Here we observe magnetic field induced circular dichroism. We measure the total fluorescence intensity as dependent on the scanned diode laser frequency (leser-induced-fluorescence excitation spectra) for both Rb isotopes. Excitation with circularly polarized as well as linearly polarized radiation is used. It is demonstrated that the laser-induced fluorescence excitation spectra is qualitatively very different for left and right circularly polarized radiation. In contrast, the corresponding Doppler broadened spectra changes only slightly as the light helicity changes and this change may be explained with a simple model that ignores the rich physics observed in the sub-Doppler spectra.

The paper is organized as follows. In Section II the experimental procedure and obtained results are presented for the two naturally occurring Rb isotopes. Section III compares the observed spectra with model calculations. In Section IV results are discussed, and in Section V conclusions are drawn.

II. EXPERIMENTAL

The design of the ETC is presented in Fig. 1. It is a new modification of sapphire cells developed earlier (see [16] and references therein). The windows of 30 mm diameter and 3 mm thickness are made from very well-polished garnet (YAG) crystal, which is resistant to highly corrosive alkaline vapors. The roughness of the inner surfaces of the YAG windows is $< \lambda/10$. In order to realize a wedged gap between the YAG windows, a 1 mm-wide and 10-mm-long Al_2O_3 strip coating of ≈ 600 nm thickness has been deposited on the surface of one of the YAG windows, near the lower edge. The sapphire side arm with a molybdenum glass termination is used for filling the cell with Rb in the same way as for all-glass cells. To attach the side arm, a hole is drilled at the bottom of the YAG windows. Before filling the ETC with natural mixture of rubidium atoms (72.15% of ^{85}Rb with nuclear spin $I = 5/2$ and 27.85% of ^{87}Rb with nuclear spin $I = 3/2$), the cell was carefully out-gassed.

The wedged gap between the windows allows us to exploit a $\sim \lambda/2$ thickness of a vapor layer that is important for having the narrowest sub-Doppler line width [14]. An interferometric mapping of the gap thickness is performed using He-Ne laser. This measurement shows that the thickness of the gap varies in the range of 100 nm - 600 nm. A ~ 400 nm thickness region of the cell aperture ($\approx \lambda/2$) has been explored in present experiment.

The upper temperature limit for the ETC is ~ 400 °C. The ETC operated with a specially designed oven, which has four openings; two for the laser beam transmission and two that allow for fluorescence to be detected simultaneously from two different directions. The density of the Rb atomic vapor is determined by the temperature of the boundary of Rb metal column inside the side arm (Fig 1). The typical value of metal boundary (side arm) temperature is kept at 120 °C throughout the measurements, while the window temperature is set to somewhat higher value (140 °C) to prevent Rb condensation. The corresponding number density of Rb atoms is $N_{Rb} \approx 2 \times 10^{13}$ cm^{-3}, and the collisional broadening is ~ 3 MHz. The Doppler line width in an ordinary cell at this temperature regime is ≈ 600 MHz.

The ETC with Rb atoms is placed in 3 pairs of mutually perpendicular Helmholtz coils which cancel the ambient magnetic field and provide a homogeneous magnetic field in an arbitrary direction. The geometry of the experiment is depicted schematically in Fig. 5. The collimated radiation beam of the cw laser diode ($\lambda = 780.2$ nm, 25 MHz line width, single mode, $\oslash$ 3 mm.) is directed at normal incidence into the Rb-filled ~ 400-nm-thick region of

the ETC. The maximum laser intensity is 50 mW/cm^2. A Glan-Thomson prism is used to purify the linear radiation polarization of the laser. To produce a circular polarization, a $\lambda/4$ plate is utilized. A photodiode with an aperture of 1 cm^2 is placed at 90° to the laser propagation direction to detect the fluorescence signal emerging through one of the two side openings of the cell oven. The photodiode collects emission within ~ 0.1 srad solid angle. The signal of the photodiode is amplified and recorded with a storage oscilloscope. The intensity of the fluorescence emission (with no spectral and polarization resolution) from the vapor layer excited by linearly and circularly polarized radiation is recorded versus the laser radiation frequency. To obtain the laser-induced-fluorescence excitation spectra, the laser frequency is scanned linearly in a 9 GHz spectral region around the Rb D_2 line by means of injection current ramping.

As a result of hyperfine interactions, the ground state level of ^{85}Rb is split into two components with total angular momentum quantum numbers $F_g = 2$ and $F_g = 3$ and the ground-state level of ^{87}Rb is split into two components with total angular momentum quantum numbers $F_g = 1$ and $F_g = 2$. The ground state level splitting for ^{85}Rb and ^{87}Rb are approximately 3 and 7 GHz, respectively. In contrast, the four excited-state hyperfine components are separated by only several hundred MHz (see Figs. 2 and 3). Since the separation of the hyperfine sub-levels of the $5P_{3/2}$ state with $F_e = 0{-}3$ for ^{87}Rb (72−157−267 MHz) and $F_e = 1 - 4$ for ^{85}Rb ($29 - 63 - 121$ MHz) is less than the Doppler broadening ($\sim$ 600 MHz), the D_2 spectrum for an ordinary Rb cell consists of only two resolved lines for each Rb isotope: $5S_{1/2}$ $(F = 1) \rightarrow$ $5P_{3/2}$ $(F = 0{-}2)$ and $5S_{1/2}$ $(F = 2) \rightarrow$ $5P_{3/2}$ $(F = 1{-}3)$ for ^{87}Rb and $5S_{1/2}$ $(F = 2) \rightarrow$ $5P_{3/2}$ $(F = 1 - 3)$ and $5S_{1/2}$ $(F = 3) \rightarrow$ $5P_{3/2}$ $(F = 2 - 4)$ for ^{85}Rb. The total laser-induced-fluorescence excitation spectra on a full D_2 line scan in the absence of the magnetic field are presented in figure 4. The gray curve shows the Doppler broadened spectrum in an ordinary room-temperature cm-long cell. The black curve shows the same spectrum in an ETC. In the latter, features representing hyperfine levels of the excited state can be seen clearly.

To explore magneto-optical effects, we register the fluorescence spectra for three different polarizations of laser radiation. Namely, left- and right- handed polarization for the case of laser propagation parallel to the magnetic field direction (σ^+ and σ^-) and linear polarization along the magnetic field direction (π). Our choice of laser radiation polarization and magnetic field direction is determined by the fact that for each of these geometries, only one

well defined transition type between magnetic sublevels of ground state m_{F_g} and magnetic sublevels of excited state m_{F_e} can take place. Namely $\Delta m = m_{F_e} - m_{F_g}$ is equal to $+1$ for σ^+ excitation, is equal to -1 for σ^- excitation, and is equal to 0 for π excitation. We record experimental laser-induced-fluorescence excitation spectra of Rb atoms at a B-field strength of 50 G. This intermediate field strength is chosen so that the Pashen - Back effect is important. At this interesting field strength, the magnetic field starts to decouple the nuclear spin **I** from the electronic angular momentum **J** but these moments still remain partially coupled. As a rule at this field strength crossing take place in the magnetically shifted hyperfine levels (see Figs. 2 and 3.)

In Figures 6, 7, 8, 9 scattered circles depict experimentally obtained signals for the following transitions ^{85}Rb, absorption $F_g = 2 \rightarrow F_e = 1, 2, 3, (4)$; ^{85}Rb, absorption $F_g = 3 \rightarrow F_e = (1), 2, 3, 4$; ^{87}Rb, absorption $F_g = 1 \rightarrow F_e = 0, 1, 2, (3)$ and ^{87}Rb, absorption $F_g = 2 \rightarrow F_e = (0), 1, 2, 3$. For reference in the same figures with lighter color are depicted experimentally measured fluorescence spectra in absence of the magnetic field. We note the observation of transitions that violate the $\Delta F = 0, \pm 1$ selection rule for electric dipole transitions. This selection rule is strictly true only for hyperfine levels in absence of the magnetic field. As the magnetic field intensity increases from zero, the hyperfine levels mix and transitions that are forbidden in absence of the field start to be allowed. The excited-state quantum number for transitions that are not allowed in the absence of a magnetic field are written in parenthesis.

From the figures presented it is clearly seen that laser-induced-fluorescence excitation spectrum for left and right-handed excitation are qualitatively different. From simple symmetry considerations, these spectra must coincide in absence of the magnetic field. In presence of the field helicity of the laser polarization with respect to the field direction starts to play a very important role and these spectra are very different for all transitions presented. In agreement with nearly linear fluorescence intensity dependence when the intensity of the diode laser is increased, reported in [16], also in case of Rb the shape of fluorescence spectrum does not noticeably depend on laser radiation intensity, at least in the range of $I_L = 1 - 50$ mW/cm^2. All the spectra presented in graphs were recorded with $I_L = 50$ mW/cm^2.

It is interesting to compare these spectra for case of ordinary cells when only Doppler broadened spectra can be recorded. In figure 10 absorption spectra obtained at room temperature in an ordinary call containing pure isotopes of Rb atoms. In one case ^{85}Rb and

in other case ^{87}Rb. Unfortunately, for technical reasons only the absorption and not the laser-induced-fluorescence excitation spectra were taken. Nevertheless, in these cells absorption and laser-induced-fluorescence excitation spectra should be very similar. We see that in these Doppler broadened spectra, both isotopes lead to spectra that are qualitatively similar for both circularities of laser radiation. Each isotope leads to only one peak for absorption from each of ground state hyperfine levels. This peak is shifted for two excitation light polarizations on a frequency scale. This peak shifting is the phenomena that the diode-laser-stabilization schemes [21, 22, 23] mentioned in the introduction exploit.

As we can see from Figs.6, 7, 8, 9, the transitions between individual magnetic sublevels $m_{Fg} \rightarrow m_{Fe}$ of the same hyperfine transition $F_g \rightarrow F_e$ are not resolved in the conditions of present experiment. Indeed, in the case of complete resolution, one would expect to up to 9 transitions between different magnetic sublevels in case of circularly polarized excitation for $F_i = 1 \rightarrow F_e = 0, 1, 2, (3)$ (cases (b) and (c) Fig. 8) and up to 22 magnetic transitions for case of linearly polarized excitation for $F_i = 3 \rightarrow F_e = (1), 2, 3, 4$ (case (a) Fig. 7). The results of this experiment can be rather interpreted as B-field dependent frequency shift and variation of probabilities of the $|F_g, m_g\rangle \rightarrow |F_e, m_e\rangle$ hyperfine transitions. In the present experiment an essential limitation for the resolution comes from the width of excitation laser line which was equal to 25 MHz. This allows to hope that in future resolution of sub-Doppler spectroscopy in ETC can be increased and can be close to the homogeneous line width of atomic transitions.

III. LASER-INDUCED-FLUORESCENCE EXCITATION SPECTRA IN A MAGNETIC FIELD. SIGNAL SIMULATION

As we see from the observed signals, there exists a well pronounced structure in laser-induced-fluorescence excitation spectra. This structure changes when the magnetic field is applied. It can not be observed in Doppler broadened spectra. Similar structure was observed earlier by [27] but only in an extremely strong magnetic field with strength of the order of 1000 G and stronger. At this field strength electronic angular momentum **J** of an alkali atom is decoupled from the nuclei spin angular momentum **I** and both angular momenta interact with external field practically independently. In present study, **J** and **I** are only partially decoupled, and we can observe Pashen – Back effect.

To simulate fluorescence spectra of Rb atoms in a magnetic field of intermediate strength we will use the following model. We will assume that laser radiation is weak and absorption rate Γ_p is small in comparison with the relaxation rates in ground and excited states, denoted by γ and Γ respectively; $\Gamma_p < \gamma, \Gamma$. This assumption is well justified by the observation that laser-induced-fluorescence excitation spectrum is independent of the laser intensity.

The Hamilton operator of the atom in a magnetic field can be written as

$$\widehat{H} = \widehat{H}_0 + \widehat{H}_{HFS} - \mu_J \cdot \mathbf{B} - \mu_I \cdot \mathbf{B}. \tag{1}$$

where $\widehat{H}_0$ is a Hamiltonian operator of unperturbed atom without taking into account nuclei spin, $\widehat{H}_{HFS}$ represents hyperfine interaction. The remaining two terms represent interaction of the electronic magnetic moment μ_J of atom and the nucleus magnetic moment μ_I with the external magnetic field $\mathbf{B}$. These magnetic moments are connected with the respective electronic and spin angular moments $\mathbf{J}$ and $\mathbf{I}$ of the atom

$$\mu_J = -\frac{g_J \mu_B}{\hbar}\mathbf{J}, \qquad \mu_I = -\frac{g_I \mu_0}{\hbar}\mathbf{I}, \tag{2}$$

where μ_B and μ_0 are the Bohr and nuclear magnetons respectively and g_J, g_I are electrotonic and nuclear Lande factors. The action of the magnetic field on the atom has two closely related effects. First, magnetic sublevels of the hyperfine levels are mixed by the magnetic field:

$$|\gamma_k m\rangle = \sum_{F_e=J_e-I}^{F_e=J_e+I} C^{(e)}_{kF_e}(B,m)\,|F_e, m\rangle\,, \qquad |\eta_j \mu\rangle = \sum_{F_g=J_g-I}^{F_g=J_g+I} C^{(g)}_{jF_g}(B,\mu)\,|F_g, \mu\rangle\,, \tag{3}$$

where $C^{(e)}_{kF_e}(B,m)$ and $C^{(g)}_{jF_g}(B,\mu)$ are mixing coefficients that depend on the field strength and magnetic quantum number m or μ. The second effect is deviation of the Zeeman magnetic sublevel splitting in the magnetic field for each hyperfine level from the linear one. It means that the additional energy of the magnetic sublevel obtained in the magnetic field is not any more linearly proportional to the field strength. New atomic states $|\gamma_k m\rangle$ and $|\eta_j \mu\rangle$ in the magnetic field in a general case are a linear combination of all initial hyperfine levels (4 in case of Rb atoms in the $5P_{3/2}$ state and 2 in case of Rb atom in the $5S_{1/2}$ state). As it is seen from Eq. (3), in the magnetic field hyperfine angular momentum quantum number F ceases to be a good quantum number, but magnetic quantum numbers m and μ are still good quantum numbers. This reflects the symmetry of the perturbation imposed by

the magnetic field and means that only hyperfine sublevels with the same magnetic quantum numbers are mixed by the magnetic field.

The mixing coefficients $C^{(e)}_{kF_e}(B,m)$ and $C^{(g)}_{jF_g}(B,\mu)$ of the hyperfine states in the magnetic field and energies of these levels in the field ${}^{\gamma_k}E_m$, ${}^{\eta_j}E_\mu$ can be found as eigenvectors and eigenvalues of the Hamilton matrix (1). In Figures 2 and 3 the energy levels obtained by the Hamilton matrix diagonalization for two Rb atom isotopes in the excited $5P_{3/2}$ state in the magnetic field are presented.

For Rb atoms in the ground state hyperfine level splitting is larger than in an excited state. It is around 3 or 7 GHz for two ^{85}Rb and ^{87}Rb isotopes respectively, see Fig. 4, which in both cases is large in comparison to the magnetic sublevel energies obtained in the magnetic field of 50 G. As a result ground state energy levels in the magnetic field can, to a very good level of approximation, be represented by the linear Zeeman effect. Namely, ${}^{\eta_j}E_\mu = g_{\eta_j}\mu_B B\mu/\hbar$, where g_{η_j} is the Lande factor of the respective hyperfine level. For very weakly mixed levels it still can be represented with the hyperfine quantum number F_g. For ^{85}Rb atoms in $5S_{1/2}$ state we have $g_{\eta_j} = -1/3$ for $F_g = 2$ and $g_{\eta_j} = 1/3$ for $F_g = 3$, and for ^{87}Rb in $5S_{1/2}$ state we have $g_{\eta_j} = -1/2$ for $F_g = 1$ and $g_{\eta_j} = 1/2$ for $F_g = 2$. In case of mixing of only two hyperfine levels the Breit-Rabi formula can be used to find both mixing coefficients and level energies (see for example [35, 36].)

In the magnetic field excited state density matrix created by the laser light can be written as (see for example [37].)

$$ {}^{kl}f_{mm'} = \frac{\widetilde{\Gamma}_p}{\Gamma + i^{kl}\Delta\omega_{mm'}} \sum_{j\mu} \langle\gamma_k m|\, \widehat{\mathbf{E}}^*_{exc}\cdot\widehat{\mathbf{D}}\,|\eta_j\mu\rangle \,\langle\gamma_l m'|\, \widehat{\mathbf{E}}^*_{exc}\cdot\widehat{\mathbf{D}}\,|\eta_j\mu\rangle^* . \tag{4} $$

and ${}^{kl}\Delta\omega_{mm'} = ({}^{\gamma_k}E_m - {}^{\gamma_l}E_{m'})/\hbar$ is the energy splitting of the magnetic sublevels m and m' belonging to the excited state levels k and l. Magnetic quantum numbers of the ground state level η_j are denoted by μ and magnetic quantum numbers of the excited state level $\gamma_{k,l}$ by m and m'. In this last expression it is assumed that two magnetic sublevels of the excited state, that initially belonged to two different hyperfine levels at some specific magnetic field strength, can have the same energy and can be excited simultaneously and coherently. It means nonzero field level crossing signals [37] in general can be included in this model. At the same time for practical calculations performed in this work this is not important, as far as laser radiation used to excite atoms in this work is chosen in such a way that it can

be represented only by one component in a cyclic system of coordinates and is not able to create coherence between magnetic sublevels of the atom.

In our particular simulation we assume that when we scan laser frequency only those transitions that are in an exact resonance with the laser field are excited. So at each laser frequency a specific density matrix is calculated. This density matrix is of course dependent on the magnetic field strength that determines magnetic sublevel splitting and wave function mixing. The intensity of the fluorescence with a specific polarization $\mathbf{E}_{obs}$ in a transition between excited γ_k and final η_j state in the magnetic field can be calculated according to [37]

$$I\left(\mathbf{E}_f\right) = I_0 \sum_{mm'\mu} \sum_{klj} \left\langle \gamma_k m \right| \widehat{\mathbf{E}}^*_{obs} \cdot \widehat{\mathbf{D}} \left| \eta_j \mu \right\rangle \left\langle \gamma_l m' \right| \widehat{\mathbf{E}}^*_{obs} \cdot \widehat{\mathbf{D}} \left| \eta_j \mu \right\rangle^{*kl} f_{mm'}. \tag{5}$$

The final state of the transition may or may not coincide with the atomic hyperfine ground state level from which the absorption started. When in expressions for excited state density matrix elements (Eq (4)) and fluorescence intensity (Eq (5)) ground $|\gamma_k m\rangle$ and excited state $|\eta_j \mu\rangle$ wave function expansion over the atomic wave functions in absence of magnetic field is used, see Eq. (3) matrix elements of the type $\langle F_e m| \widehat{\mathbf{E}}^*_{exc} \cdot \widehat{\mathbf{d}} \, |F_g \mu\rangle$ appear. Standard methods of angular momentum theory can be used to calculate these matrix elements, see for example [31, 32, 33, 34].

IV. ANALYSIS

For laser-induced-fluorescence excitation spectra simulation in a magnetic field we use the following procedure. From the magnetic sublevel energy spectra obtained from the Hamilton matrix diagonalization we calculate absorption line positions in a magnetic field. Then we calculate absorption line strengths for these transitions taking into account level mixing, the specific laser radiation polarization, and the magnetic field value. Then we assume that the predominant factor in the formation of the absorption line shape is homogeneous broadening. In the general case the profile is a Voigt contour which is a convolution of homogeneous (Lorentzian) and inhomogeneous (Gaussian) line shapes [38]. Our assumption that inhomogeneous broadening is substantially reduced in a sum-micron cell allows us to employ a Lorentzian absorption profile. From the energy levels, intensities, and line profiles, we are able to create spectra of expected fluorescence intensity in the absence of spectral

and polarization discrimination, but with specific emission directions. It means that in this way we are simulating laser-induced-fluorescence excitation spectra for our excitation – observation conditions.

In Figures 6, 7, 8, 9 calculated intensities of fluorescence are shown as vertical bars of heights that represent the intensity of fluorescence at a specific laser excitation frequency. Solid lines in figures show laser-induced-fluorescence excitation spectra that takes into account the linewidth of each absorption line as described above. To get the best coincidence between measured and calculated spectra the homogeneous linewidth of each absorption component was assumed to be equal to 45 MHz. This is several times the natural linewidth of the resonant transition of unperturbed Rb atom. The radiation width of the absorption components in D_2 line are expected to be approximately $\Delta\nu_{D_2} = 1/(2\pi\tau) \approx 6$ MHz [30], where $\tau \approx 26$ ns is lifetime of Rb in $5P_{3/2}$ state. Partially this absorption line broadening is due to the fact that we have a broad laser line – 25 MHz. The rest of the broadening of the absorption line most probably can be attributed to the atomic collisions within the cell walls.

V. CONCLUSIONS

For the first time it was demonstrated that ETC can be successfully used to study spectra with sub-Doppler resolution of alkali atoms in a magnetic field. In particular, for rather weak magnetic field of 50 G when nucleus spin angular momentum **I** and electronic angular momentum **J** are only partially decoupled, we registered changes in laser-induced-fluorescence excitation spectrum with sub-Doppler resolution of Rb atoms when different polarizations of excitation laser are used. It was demonstrated that spectra when right- and left-hand circularly polarized excitation is used differ very strongly and these differences are not only quantitative, but also qualitative. A strong magnetic field induced circular dichroism in this experiment is clearly observed. Appearance of this circular dichroism may be explained in a standard approach which describes how partial decoupling of **I** and **J** mixes together magnetic sublevels of different hyperfine states of alkali atoms. As a result we have a nonlinear Zeeman effect for each magnetic sublevel. A second consequence of this mixing of wave functions of different hyperfine states is a substantial modification of transition probabilities between different magnetic sublevels, including the fact that transitions that are

strictly forbidden in absence of the magnetic field start to be allowed. The importance of these changes of transition probabilities even for the case of a rather weak magnetic field illustrates that thin cells can show a sensitivity to physical processes not accessible to conventional spectroscopy.

VI. ACKNOWLEDGMENTS

The authors are very thankful to Prof. Neil Shafer-Ray for fruitful discussions. The authors are grateful to A. Sarkisyan for his valuable participation in fabrication of the ETC. This work was supported, in part, by ANSEF Grant # PS 18-01 and Armenian Republic Grants # 1351, 1323.

---

[1] A.L. Schawlow, Rev. Mod. Phys. 54(3) (1982) 697

[2] V. S. Letokhov, V.P. Chebotayev, Nonlinear Laser Spectroscopy, Springer Series in Optical Sciences, Vol. 4, Springer, Berlin, 1977

[3] R. Wynands, A. Nagel, Appl. Phys. B 68 (1999) 1

[4] D.S. Glassner, B. Ai, R.J. Knize, Opt. Lett. 19 (1994) 2071

[5] B. Ai, D.S. Glassner, R.J. Knize, J.P. Partanen, Appl. Phys. Lett. 64(8) (1994) 951

[6] S. Briaudeau, D. Bloch, M. Ducloy, Europhys. Lett. 35(5) (1996) 337

[7] S. Briaudeau, S. Saltiel, G. Nienhuis, D. Bloch, M. Ducloy, Phys. Rev. A 57 (1998) R3169

[8] S. Briaudeau, D. Bloch, M. Ducloy, Phys. Rev. A 59 (1999) 3723

[9] S. Briaudeau, S. Saltiel, J.R.R. Leite, M. Oria, A. Bramati, A. Weis, D. Bloch, M. Ducloy, J. Phys. IV France 10 (2000) Pr8-145

[10] A. Izmailov, Laser Phys. 3 (1993) 507

[11] R.H. Romer, R.H. Dicke, Phys. Rev. 99 (1955) 532

[12] T.A. Vartanyan, D.L. Lin, Phys. Rev. A 38 (1995) 5197

[13] B. Zambon, G. Nienhuis, Opt. Commun. 143 (1997) 308

[14] A. Yarovitski, G. Dutier, S. Saltiel et al. , Int. Quant. Electr. Conf. IQEC/2002, Technical Digest, p. 333, Moscow, Russia, 2002

[15] G. Dutier, S. Saltiel, D. Bloch, M. Ducloy, *to be published*

[16] D. Sarkisyan, D. Bloch, A. Papoyan, M. Ducloy, Opt. Commun. 200 (2001), 201

[17] I.B. Khriplovich, S.K. Lamoreaux, *CP Violation Withour Strangeness, Electric Dipole Moments of Particles, Atoms, and Molecules*, Springer, Berlin, Heidelberg, New York, Barcelona, Budapest, Hong Kong, London, Milan, Paris, Santa Clara, Singapore, Tokyo (1997) 230

[18] E.D. Commins, Physica Scripta 46 (1993) 92

[19] M.A. Bouchiat, C. Bouchiat, Rep. Progr. Phys. 60 (1997) 1351

[20] J. Guena, D. Chauvat, Ph. Jacquier, E. Jahier, M. Lintz, S. Sanguinetti, A. Wasan, M.A. Bouchiat, A.V. Papoyan, D. Sarkisyan, Phys. Rev. Lett., 90 (2003), 143001

[21] V.V. Yashchuk, D. Budker, J.R. Davis, Rev. Sci. Instrum. 71(2) (2000) 341

[22] M.A. Clifford, G.P.T. Lancaster, R.S. Conroy, K. Dholakia, J. Mod. Opt. 47(11) (2000) 1933

[23] K.L. Corwin, Z.T. Lu, C.F. Hand, R.J. Epstein, C.E. Wieman, Appl. Opt. 37(15) (1998) 3295

[24] V.N. Novikov, O.P. Sushkov, I.B. Khriplovich, Opt. Spectrosc. 42 (1977) 370; Opt. Spectrosc. 45 (1978) 236

[25] G.J. Roberts, P.E.G. Baird, M.W.S. Brimicombe, P.G.H. Sandars, D.R. Selby, D.N. Stacey, J. Phys. B: Atom. Molec. Phys. 13 (1980) 1389

[26] X. Chen, V.L. Telegdi, A. Weis, J. Phys. B: Atom. Molec. Phys. 20 (1987) 5653

[27] P. Tremblay, A. Michaud, M. Levesque, S. Theriault, M. Breton, J. Beaubien, N. Cyr, Phys. Rev. A 42(5) (1990) 2766

[28] A. Weis, V.A. Sautenkov, T.W. Hansch, J. Phys. II France 3 (1993) 263

[29] N. Papageorgiou, A. Weis, V.A. Sautenkov, D. Bloch, M. Ducloy, Appl. Phys. B 59 (1994) 123

[30] C.E. Theodosiou, Phys. Rev. A 30 (1984) 2881

[31] M. Auzinsh, R. Ferber, *Optical Polarization of Molecules,* Cambridge University Press, Cambridge (1995)

[32] R.N. Zare, *Angular Momentum,* J. Wiley and Sons, New York (1988)

[33] D.A. Varshalovich, A.N. Moskalev, V.K. Khersonskii, *Quantum Theory of Angular Momentum*, World Scientific, Singapore (1988)

[34] I.I. Sobelman, *Atomic Spectra and Radiative Transitions*, Springer Verlag, Berlin (1979)

[35] E.B. Aleksandrov, M.P. Chaika, G.I. Khvostenko, *Interference of Atomic States*, Springer Verlag, New York, (1993)

[36] S. Svanberg, *Atomic and Molecular Spectroscopy: Basic Aspects and Prectical Applications*,

Springer, Berlin, Heidelberg (1992)

[37] J. Alnis, M. Auzinsh, Phys. Rev. A 63 (2001) 023407

[38] W. Demtroder, *Laser spectroscopy: Basic Concepts and Instrumentation,* Springer, Berlin, Heidelberg, New York, Hong Kong, London, Milan, Paris, Tokyo (2002)

VII. CAPTIONS TO THE FIGURES

FIG. 1: The design of the ETC. 1 – the windows of the ETC, made from a garnet (YAG) crystal, the thickness is 3 mm, diameter is 30 mm. The flatness of the both inner surfaces of the YAG windows is less than $\lambda/10$; 2 – $\sim$ 600 nm-thick Al_2O_3 coating in the shape of a 1 mm-wide and 10 mm-long strip; 3 – the glue; 4 – the sapphire side arm with a "molybdenum glass" termination; 5 – column of Rb metal.

FIG. 2: Excited-state hyperfine magnetic sublevel splitting for intermediate strength of a magnetic field for ^{85}Rb isotope

FIG. 3: Excited-state hyperfine magnetic sublevel splitting for intermediate strength of a magnetic field for ^{87}Rb isotope.

FIG. 4: Doppler broadened fluorescence spectra (light line) obtained in an ordinary cell and sub-Doppler spectra obtained in ETC on D_2 line of both Rb isotopes in absence of the magnetic field.

FIG. 5: Geometrical configuration of the experiment. Magnetic field is applied along z or x axis.

FIG. 6: Experimental (scatter circle) and simulated (dark line) fluorescence spectra of ^{85}Rb isotope on transitions $F_g = 2 \rightarrow F_e = 1, 2, 3, (4)$. (a) linearly polarized π excitation, (b) circularly polarized σ^- excitation, (c) circularly polarized σ^+ excitation. With light line respective fluorescence spectra in absence of the magnetic field is shown.

FIG. 7: Experimental (scatter circle) and simulated (dark line) fluorescence spectra of ^{85}Rb isotope on transitions $F_g = 3 \rightarrow F_e = (1), 2, 3, 4$. (a) linearly polarized π excitation, (b) circularly polarized σ^- excitation, (c) circularly polarized σ^+ excitation. With light line respective fluorescence spectra in absence of the magnetic field is shown.

FIG. 8: Experimental (scatter circle) and simulated (dark line) fluorescence spectra of ^{87}Rb isotope on transitions $F_g = 1 \rightarrow F_e = 0, 1, 2, (3)$. (a) linearly polarized π excitation, (b) circularly polarized σ^- excitation, (c) circularly polarized σ^+ excitation. With light line respective fluorescence spectra in absence of the magnetic field is shown.

FIG. 9: Experimental (scatter circle) and simulated (dark line) fluorescence spectra of ^{87}Rb isotope on transitions $F_g = 2 \rightarrow F_e = 1, 2, 3, (4)$. (a) linearly polarized π excitation, (b) circularly polarized σ^- excitation, (c) circularly polarized σ^+ excitation. With light line respective fluorescence spectra in absence of the magnetic field is shown.

FIG. 10: Absorption spectra in an ordinary optical cell for (a) ^{85}Rb and (b) ^{87}Rb. Peak 1 is absorption for σ^- or σ^+ radiation in absence of the magnetic field. Peak 2 corresponds to the absorption of σ^- radiation in a magnetic field and peak 3 to the absorption of σ^+ radiation.

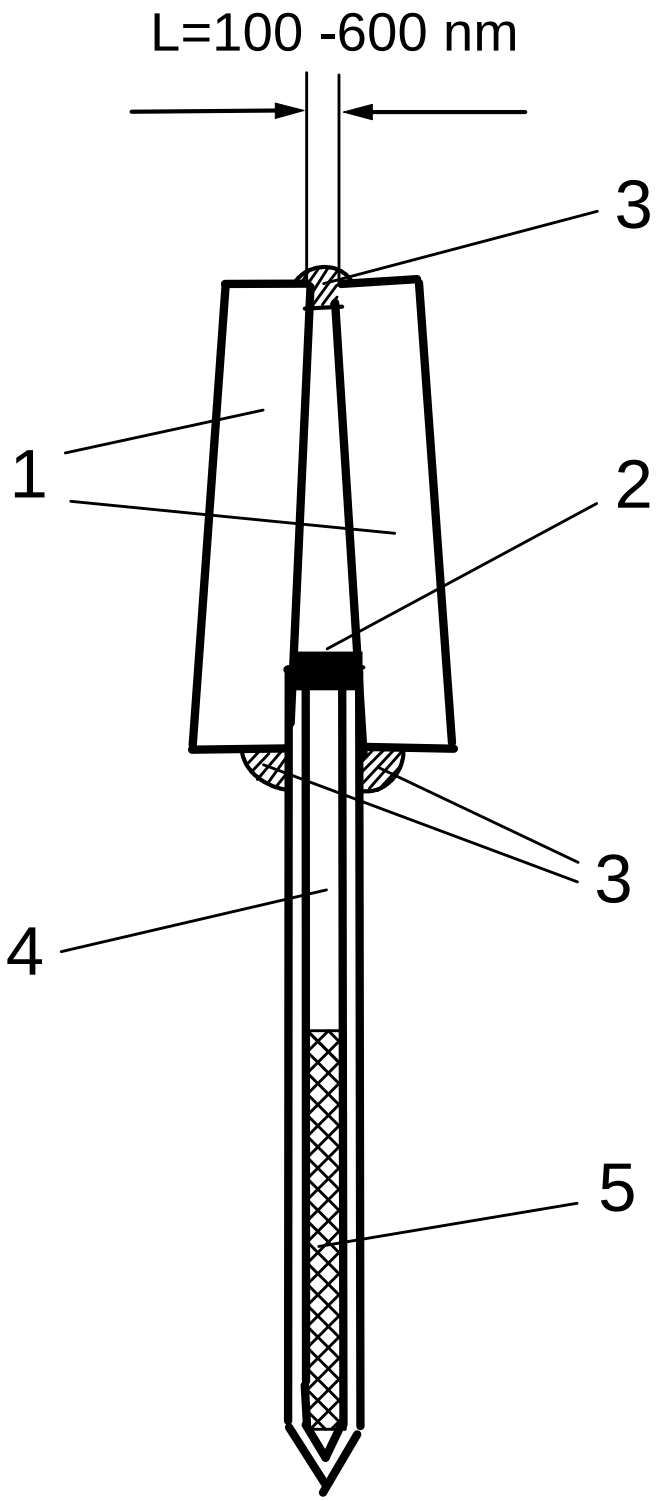

Fig. 1

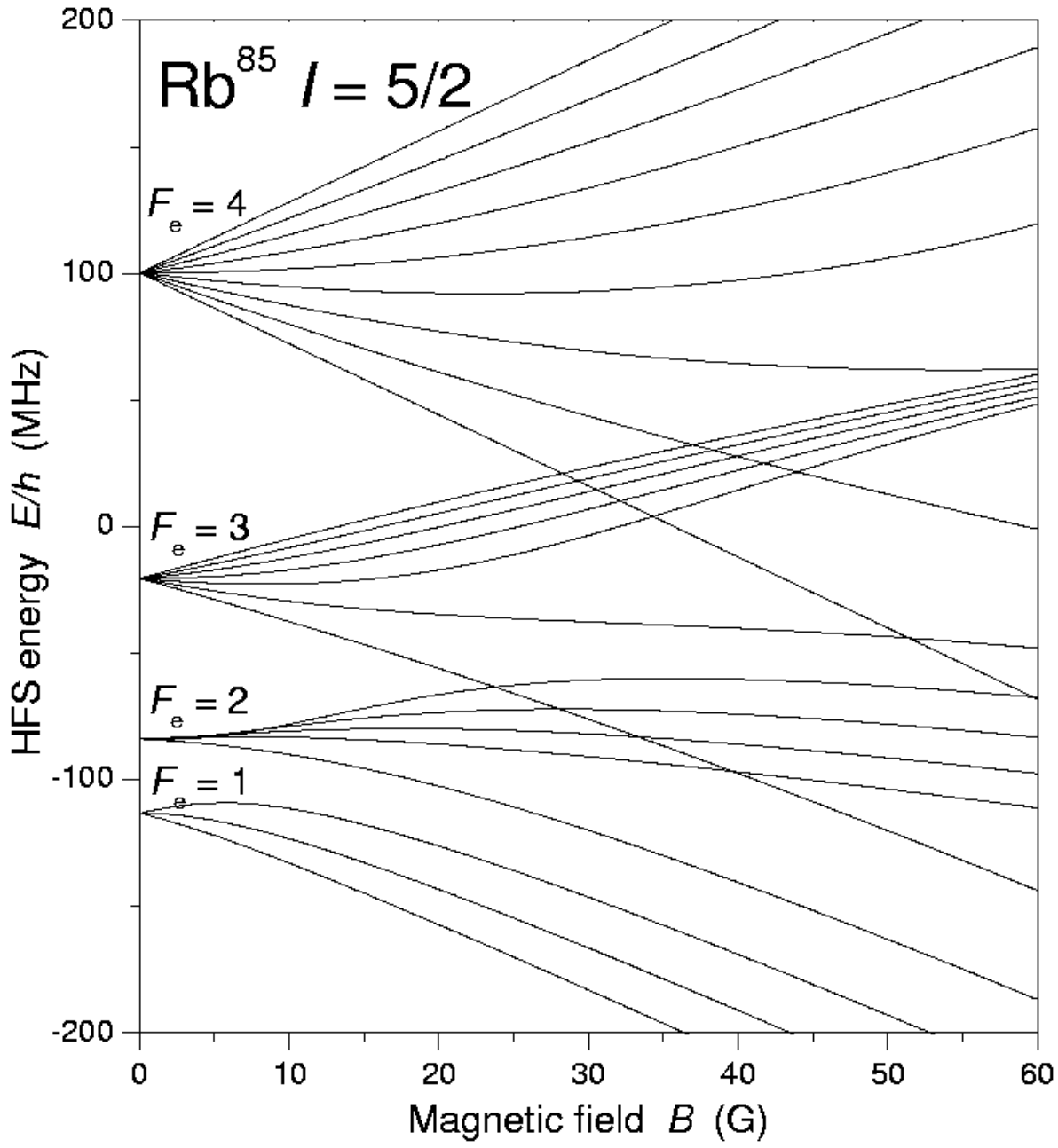
Rb85 I = 5/2
Fe = 4
Fe = 3
Fe = 2
Fe = 1
HFS energy E/h (MHz)
Magnetic field B (G)
200
100
0
-100
-200
0
10
20
30
40
50
60

Fig. 2

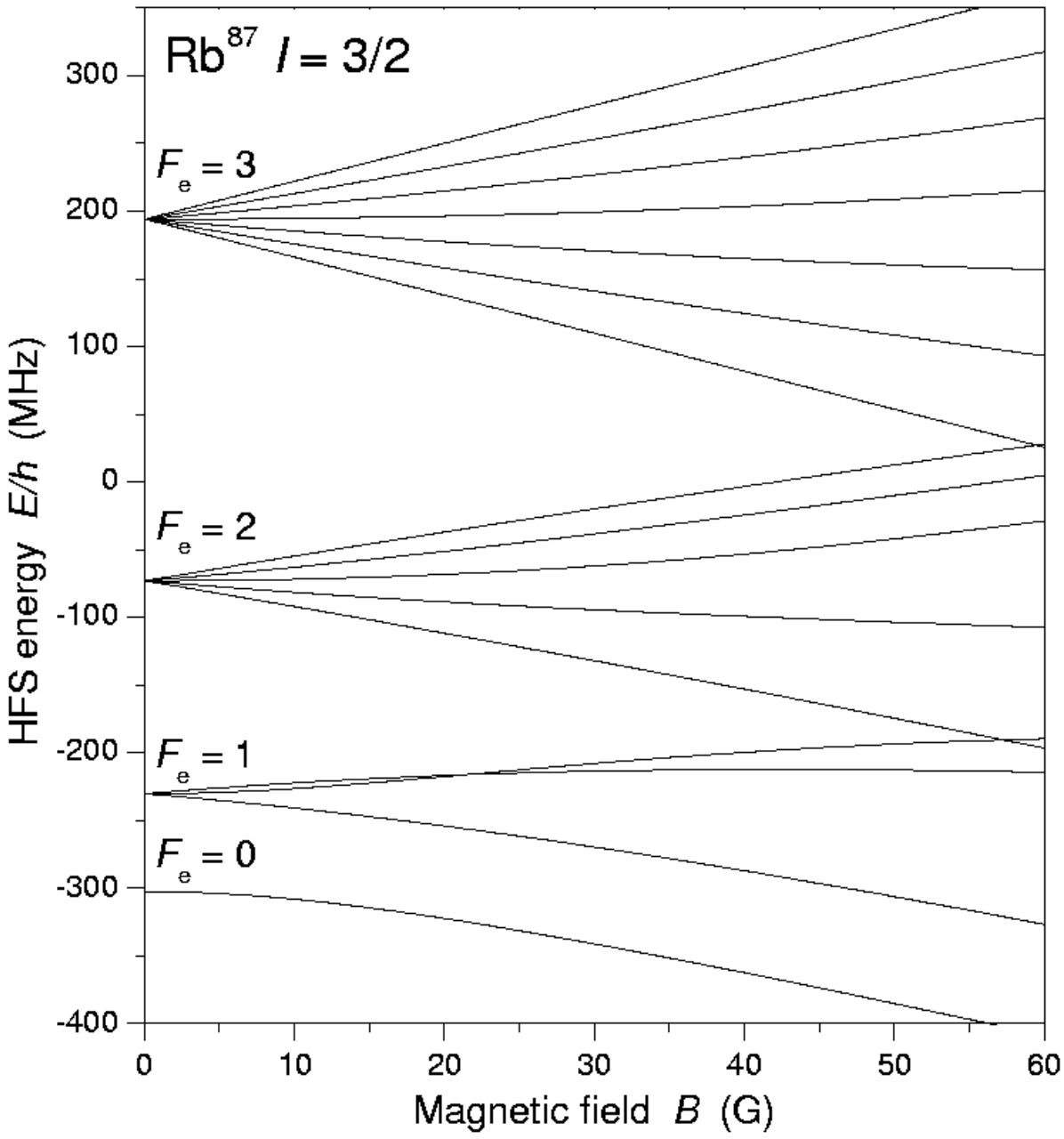
Rb87 I = 3/2
Fe = 3
Fe = 2
Fe = 1
Fe = 0
HFS energy E/h (MHz)
Magnetic field B (G)
300
200
100
0
-100
-200
-300
-400
0
10
20
30
40
50
60

Fig. 3

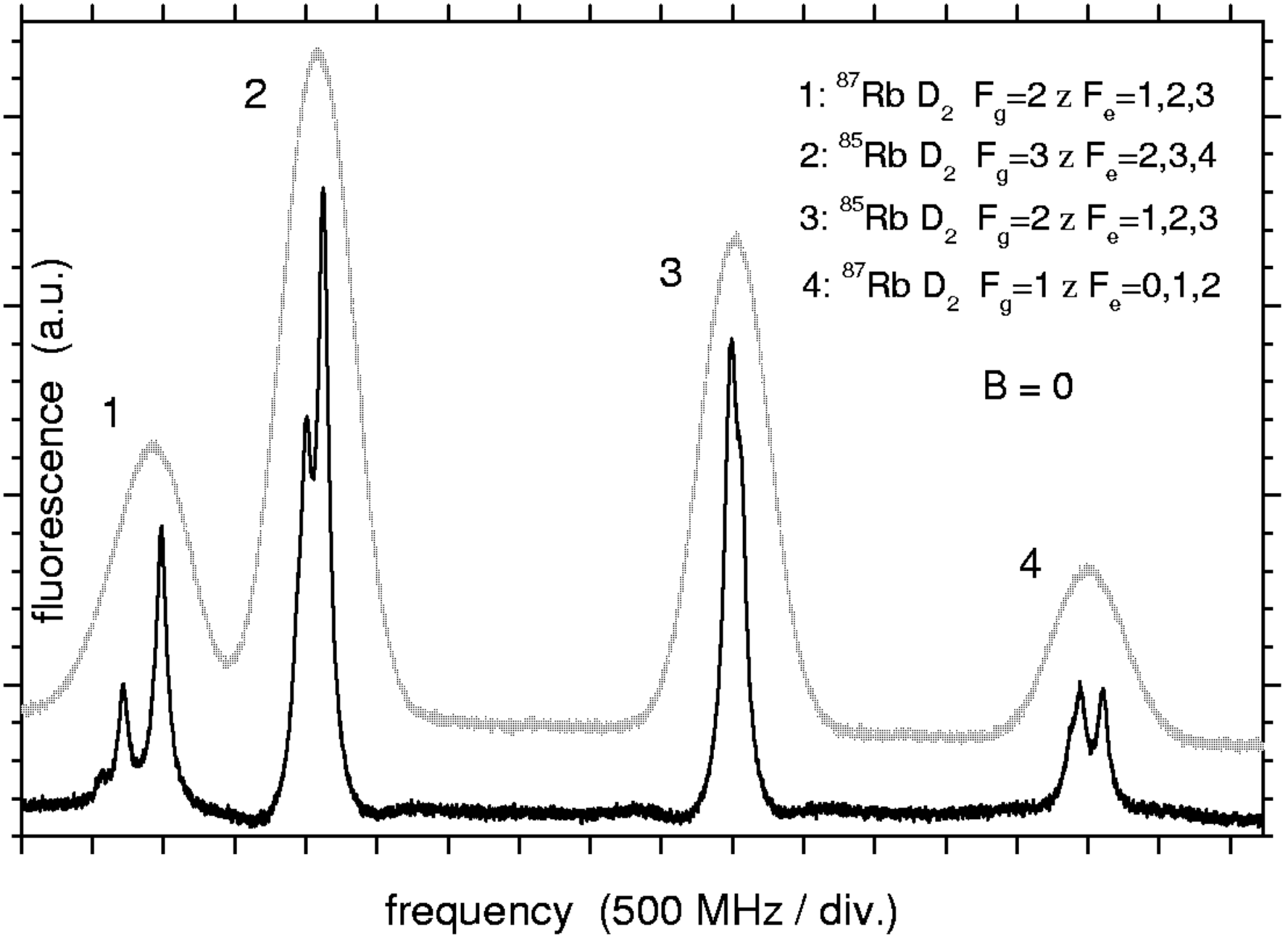
1
2
3
4
1: 87Rb D2 Fg=2 z Fe=1,2,3
2: 85Rb D2 Fg=3 z Fe=2,3,4
3: 85Rb D2 Fg=2 z Fe=1,2,3
4: 87Rb D2 Fg=1 z Fe=0,1,2
B = 0
fluorescence (a.u.)
frequency (500 MHz / div.)

Fig. 4

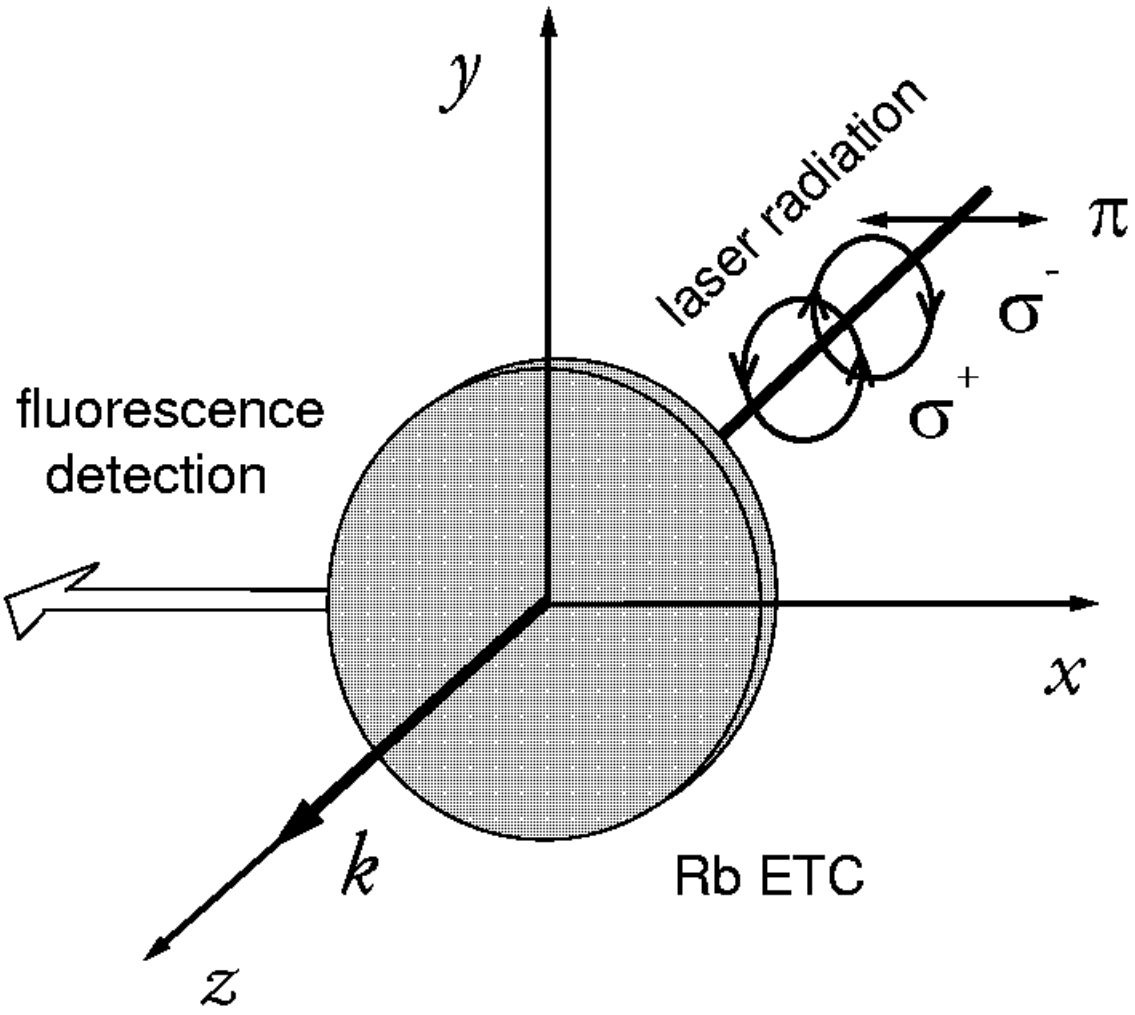

Fig. 5

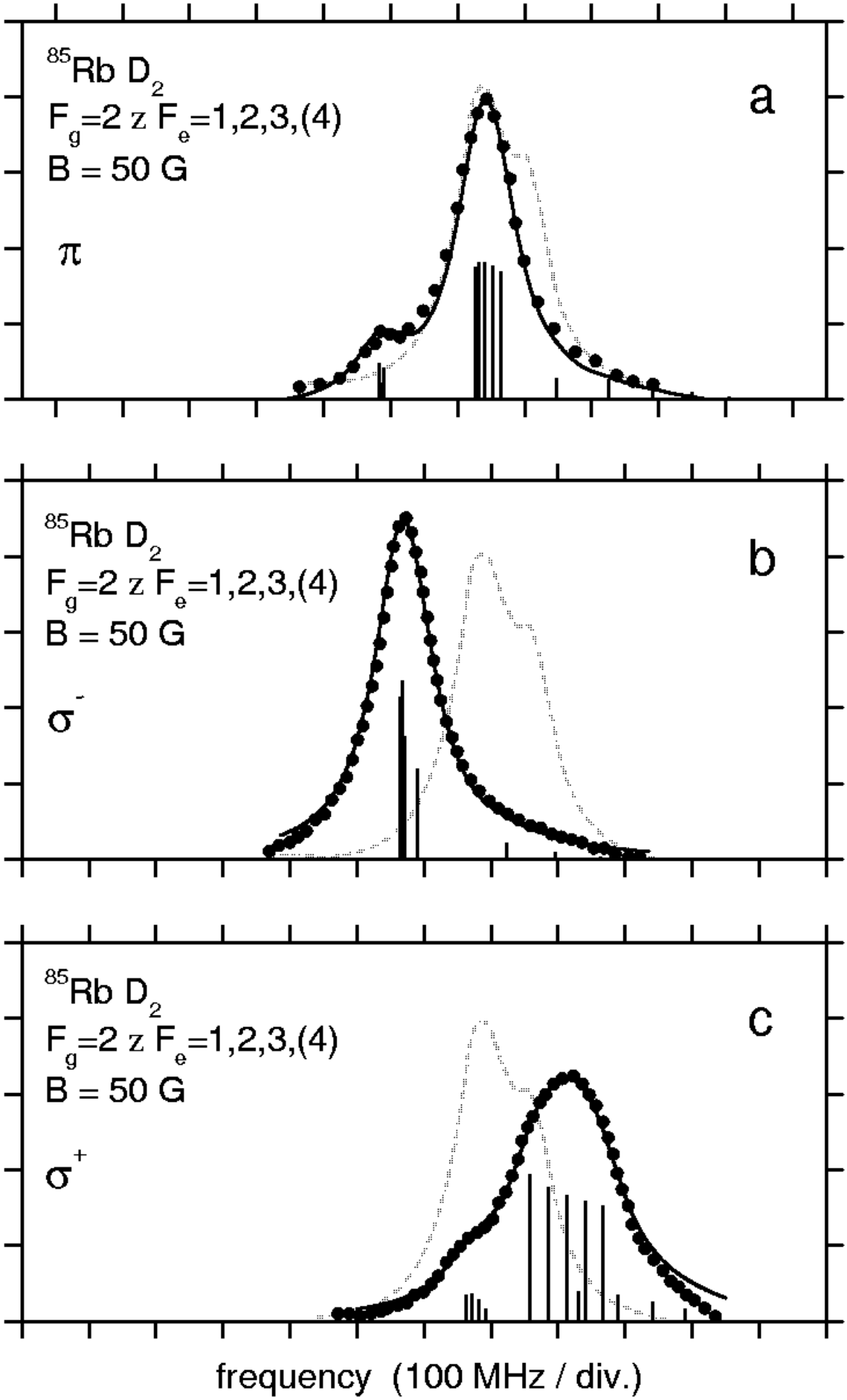
^{85}Rb D$_2$
F$_g$=2 z F$_e$=1,2,3,(4)
B = 50 G
π
a
^{85}Rb D$_2$
F$_g$=2 z F$_e$=1,2,3,(4)
B = 50 G
σ$^-$
b
^{85}Rb D$_2$
F$_g$=2 z F$_e$=1,2,3,(4)
B = 50 G
σ$^+$
c
frequency (100 MHz / div.)

Fig. 6

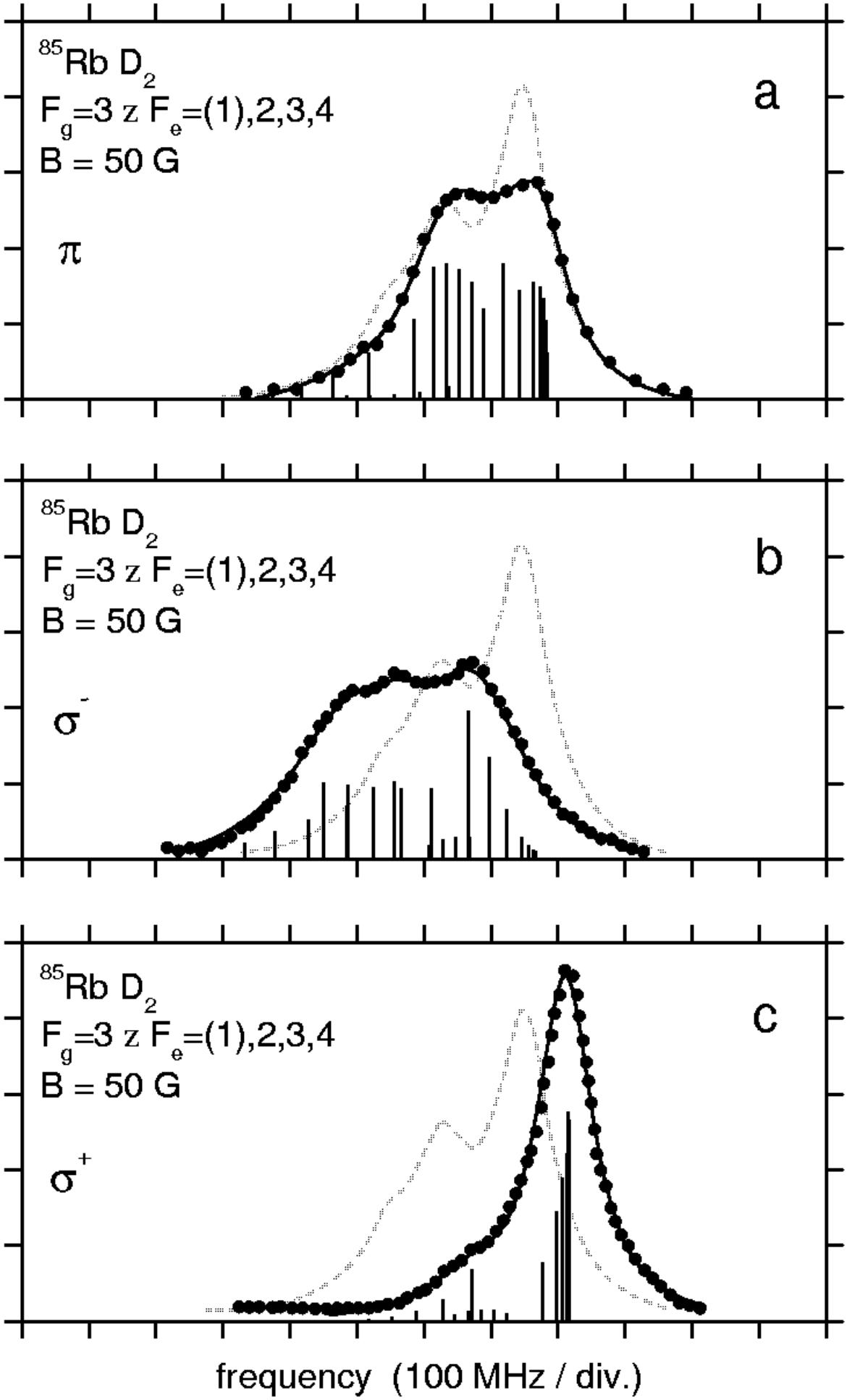
^{85}Rb D$_2$
F$_g$=3 z F$_e$=(1),2,3,4
B = 50 G
π
a
^{85}Rb D$_2$
F$_g$=3 z F$_e$=(1),2,3,4
B = 50 G
σ$^-$
b
^{85}Rb D$_2$
F$_g$=3 z F$_e$=(1),2,3,4
B = 50 G
σ$^+$
c
frequency (100 MHz / div.)

Fig. 7

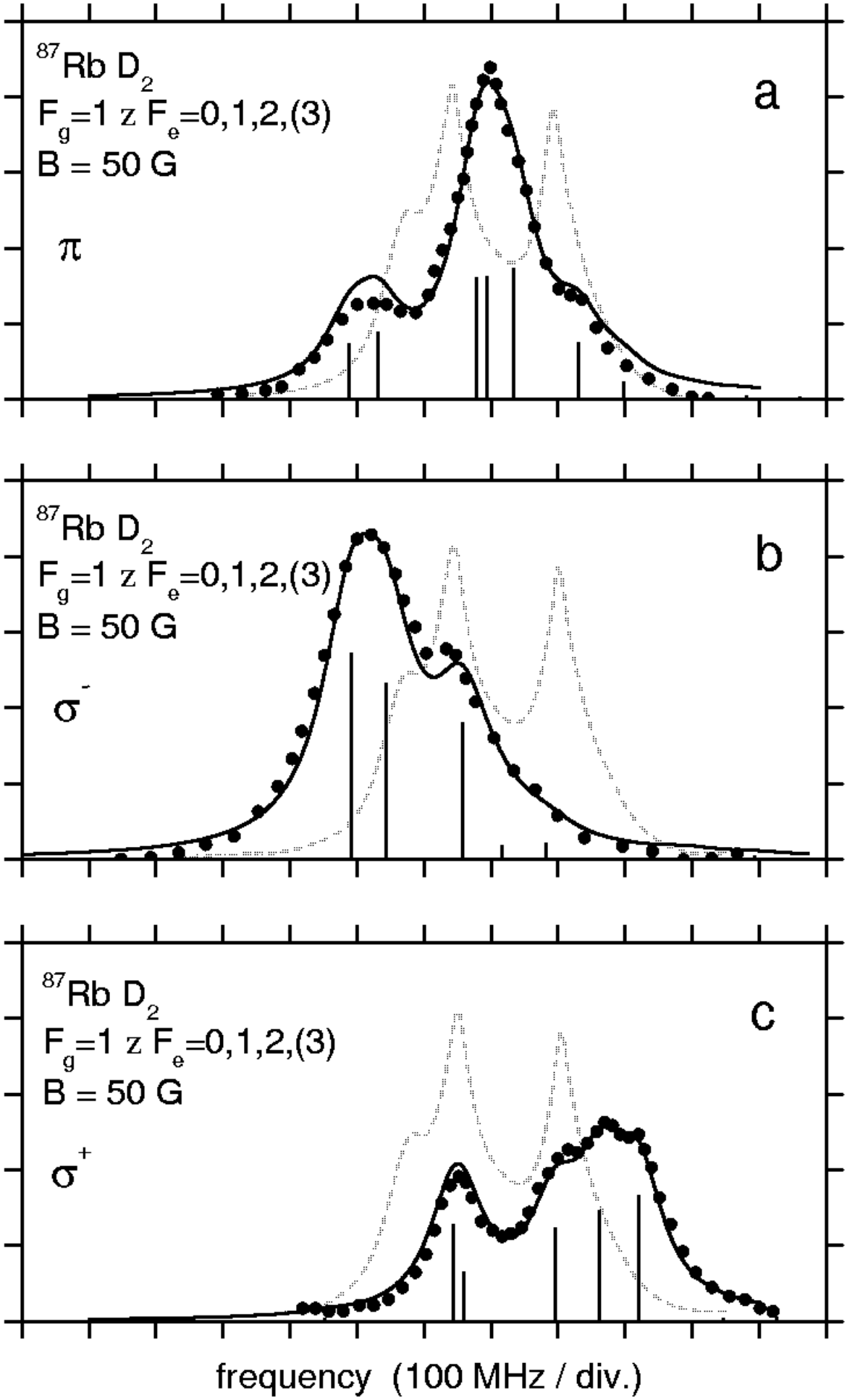
87Rb D2
Fg=1 z Fe=0,1,2,(3)
B = 50 G
π
a
87Rb D2
Fg=1 z Fe=0,1,2,(3)
B = 50 G
σ-
b
87Rb D2
Fg=1 z Fe=0,1,2,(3)
B = 50 G
σ+
c
frequency (100 MHz / div.)

Fig. 8

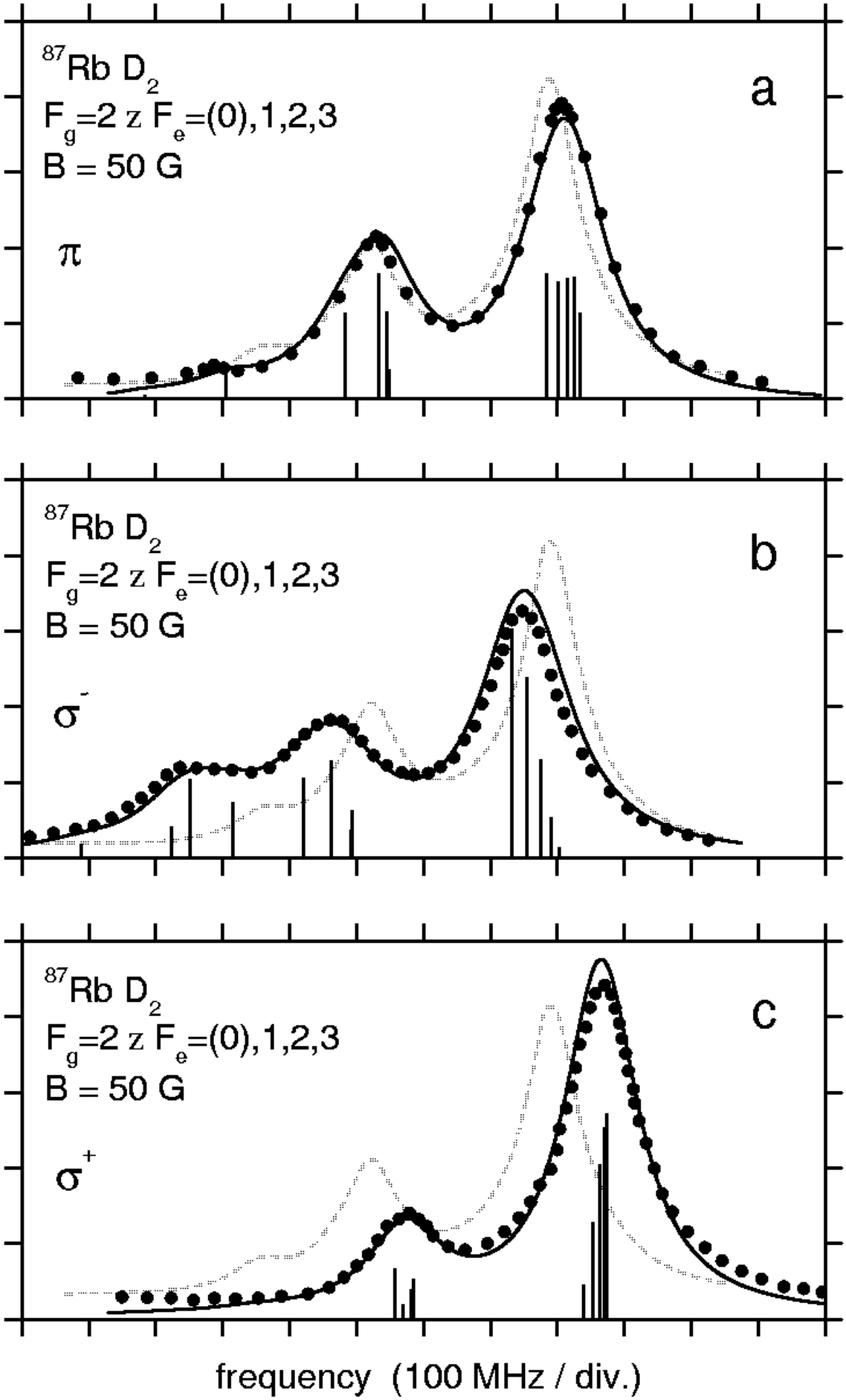
87Rb D2
Fg=2 z Fe=(0),1,2,3
B = 50 G
π
a
87Rb D2
Fg=2 z Fe=(0),1,2,3
B = 50 G
σ-
b
87Rb D2
Fg=2 z Fe=(0),1,2,3
B = 50 G
σ+
c
frequency (100 MHz / div.)

Fig. 9

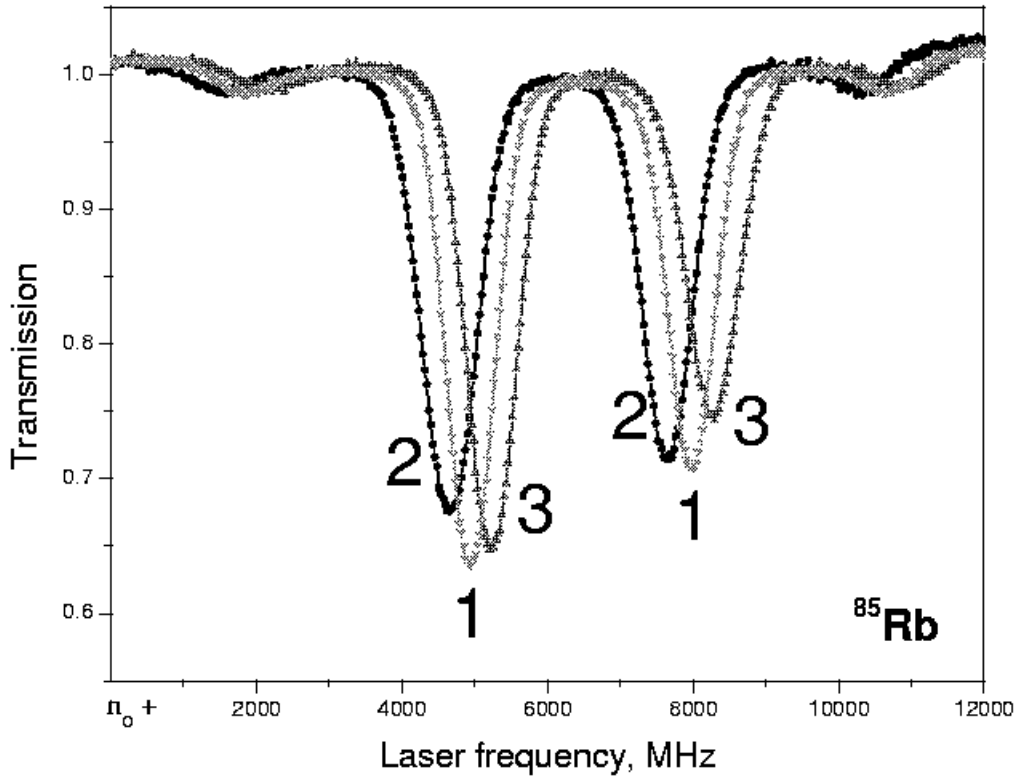
Transmission
1.0
0.9
0.8
0.7
0.6
2
3
1
2
3
1
^{85}Rb
π_o +
2000
4000
6000
8000
10000
12000
Laser frequency, MHz

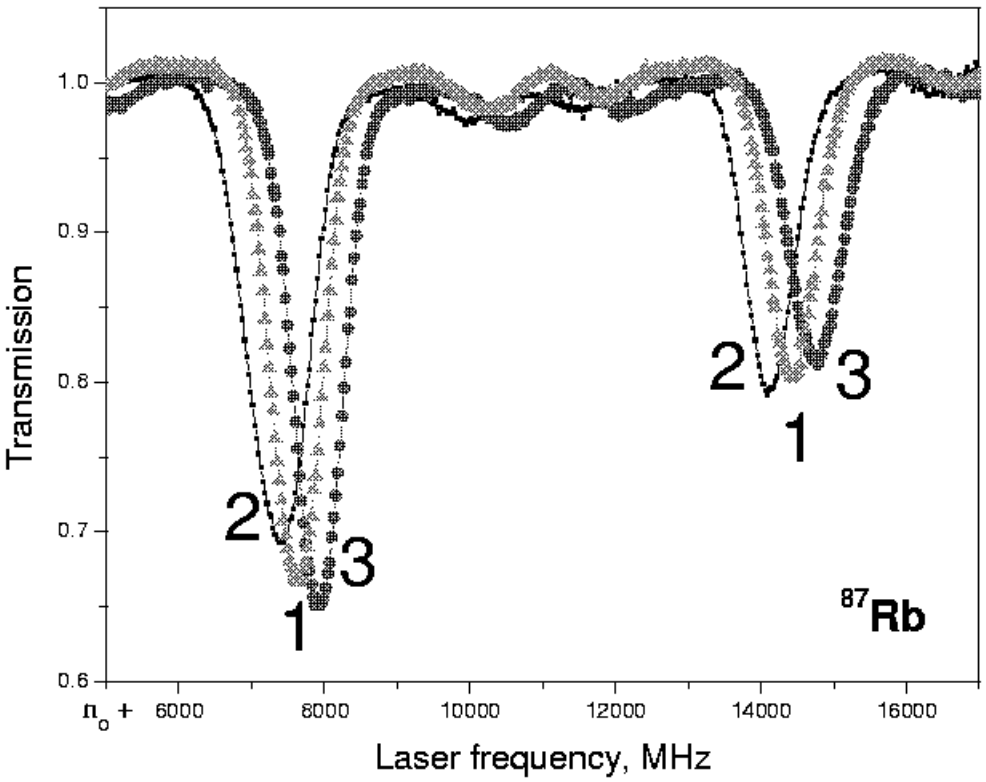
Transmission
1.0
0.9
0.8
0.7
0.6
2
3
1
2
3
1
^{87}Rb
π_o +
6000
8000
10000
12000
14000
16000
Laser frequency, MHz

Fig. 10